Hindawi
Shock and Vibration
Volume 2021, Article ID 7448439, 11 pages
https://doi.org/10.1155/2021/7448439

Research Article

Study on Thermal Effect of Nozzle Flowmeter Based on Fluid-Solid Coupling Method

Liang-Huai Tong,[1] Su-Lu Zheng,[1] Yu-Liang Zhang ,[2] Yan-Juan Zhao,[3] Kai-Yuan Zhang,[2] and Jin-Fu Li[2]

[1]*Quzhou Special Equipment Inspection Center, Quzhou 324000, China*
[2]*College of Mechanical Engineering, Quzhou University, Quzhou 324000, China*
[3]*College of Information Engineering, Quzhou College of Technology, Quzhou 324000, China*

Correspondence should be addressed to Yu-Liang Zhang; zhang002@sina.com

Received 18 July 2021; Revised 5 October 2021; Accepted 17 November 2021; Published 2 December 2021

Academic Editor: Qilong Xue

Nozzle flowmeter is widely used in industry. In this paper, in order to study the influence of different flow rates and inner wall temperatures on the thermal effect and flow field of the nozzle flowmeter, the fluid-solid coupling numerical calculation of the thermal effect and flow field of nozzle flowmeter is carried out under four different flow rates and five different inner wall temperatures. It is found that, with the increase of flow rate, the heat transfer effect of the nozzle flowmeter is weakened under different inner wall temperatures. The pressure distribution in the fluid domain, the dynamic stress, and fluid-induced vibration deformation generated by the fluid of the nozzle flowmeter are less affected by inner wall temperatures.

1. Introduction

Accurate measurement of steam plays an important role in industrial production. At present, there are two common flowmeters for measuring steam: vortex flowmeter and differential pressure flowmeter. The vortex flowmeter is mainly composed of vortex flow sensor, flow integrator, pressure transmitter, and temperature platinum thermal resistance. Differential pressure flowmeter is mainly composed of throttling device (including standard orifice, nozzle, and long diameter nozzle), differential pressure transmitter, flow integrator, pressure transmitter, and temperature platinum thermal resistance. As the most widely used steam flowmeter, orifice flowmeter also has problems such as low measurement accuracy and small measurement range [1]. The nozzle flowmeter is gradually being used more and more because it can overcome the problems of standard orifice plate in measurement. Nozzle steam flowmeter has its unique advantages in the measurement of high temperature and high pressure fluid, and it is widely used in the industrial field [2]. However, the current research on flowmeter mainly focuses on the accuracy calibration of steam flowmeter, and the analysis of fluid-solid coupling thermal effect and flow field of flowmeters is less [3–7]. The nozzle flowmeter is widely used in heat-engine plant. As we know, the media temperature inside pipes is very high, and it is 700°C sometimes. The high temperature may play an important role in internal flow. In order to reveal the effect of temperature on flow or wall of flowmeter, it is necessary to deeply study the temperature effect.

Zhang et al. proposed a dual-parameter measurement method of gasliquid two-phase flow based on a dual-cone meter. The experimental results show that it is efficient to utilize this dual-cone method for high GVF and low pressure gasliquid two-phase flow measurement [8]. Recent years, the computational fluid dynamic (CFD) method is widely used to predict the internal flow characteristics [9–12]. Chen et al. studied the effects of the aft-cone angle of the swirler on the vortex precession characteristics and pressure loss inside a swirlmeter by means of a numerical simulation and experiment [9]. The results show that the pressure pulsation at the throat is stronger than that in the convergent region, the swirling flow through the swirler is affected by different outlet velocities with various values of aft-cone angle, and the aft-cone angle directly affects both the pressure loss and vortex precession frequency of the swirlmeter. Chen et al. also found that the pressure fluctuation frequency inside has a linear response to flow rate, and the swirlmeter achieves high accuracy over a large measurement range [10]. The pressure fluctuation near the region between throat and diffusor was stronger than other regions offering then an ideal location to mount the piezoelectric sensors. Different swirler cone angles were shown to influence both pressure drop and fluctuation; smaller cone angles produced higher frequency fluctuations but larger pressure loss.

Perumal et al. studied the effect of high pressure and low pressure wet gas on internal flow. It is showed that, as the diameter increases, the influence of beta on the discharge coefficient decreases. Simulation results reveal that a convergent angle of 10.5 deg to be a better choice for wet gas metering. Homogeneous flow model, Steven's and De Leeuw's correlations are found to be better than the other correlations. While homogeneous flow model performs consistently, Steven's and De Leeuw's performance drops at 40 bar. In this paper, the influence of different flow rates and inner wall temperatures on the thermal effect and flow field of nozzle flowmeter is studied based on the CFD method and fluid-solid coupling method.

2. Physical Model and Working Principle

2.1. Geometric Model. The nozzle performance is largely affected by the internal structure and flow field distribution. The nozzle flowmeter is mainly composed of four parts: front measuring tube, rear measuring tube, nozzle, and weld metal. The specific structure and sectional view of the flowmeter are shown in Figure 1. The dimensions of measuring tube, octagonal nozzle, and weld metal are shown in Figures 2–4. The materials of measuring tube, eight groove nozzle, and weld metal are 12CrMoVG, 304 stainless steel, and H08CrMoVA, respectively.

2.2. Working Principle. The working principle is that when the fluid flows through the nozzle of the flowmeter, the fluid will shrink in the nozzle, which accelerates the flow rate and reduces the static pressure of the fluid. At this time, the pressure drop will occur before and after the nozzle. The greater the medium flow is, the greater the pressure difference will be generated before and after the nozzle. Therefore, the flow rate of the fluid can be measured by measuring the pressure difference. The two-dimensional assembly drawing of the nozzle flowmeter is shown in Figure 5. As the fluid flows through the eight-slot nozzle, it is accelerated and the kinetic energy increases. At the same time, according to the law of conservation of energy, when the fluid is accelerated, the static pressure will reduce a corresponding value, and the magnitude of the pressure drop has a certain functional relationship with the flow of the fluid. The pressure drop has a linear growth relation with the volume flow rate of the fluid. The flow rate formula is shown as follows:

$$q_v = \frac{C}{\sqrt{1-\beta_r{}^4}}\varepsilon \cdot \frac{\pi}{4} \cdot D^2 \cdot \sqrt{\frac{2\Delta p}{\rho}}, \quad (1)$$

where q_v is volume flow under working conditions (m^3/s), C is outflow coefficient, β_r is diameter ratio of throttle body, that is, the ratio of opening diameter of the throttle body to the inner diameter of the pipeline, d/D, d is the inner diameter of eight-slot nozzle under working condition (mm), D is the inner diameter of the measuring pipeline under working condition (mm). ε is the expansion coefficient of the measured medium, for incompressible fluid, $\varepsilon = 1$; gas and steam are compressible fluids, $\varepsilon < 1$; in this paper, $\varepsilon = 1$. Δp is differential pressure value before and after orifice plate (Pa), and ρ is fluid density under working conditions (kg/m^3).

The parameter Δp of formula (1) is the pressure drop after the fluid flows through the nozzle, that is, the pressure difference between the upstream and downstream of the eight-slot nozzle. In order to realize the online monitoring of the pressure difference, it is necessary to open the pressure taking orifice at the appropriate position of the front and rear pipelines connected with the nozzle.

3. 3D Model and Grid Division

The full flow field and solid structure of nozzle flowmeter are modeled in equal proportion by using 3D modeling software UG, and the hydraulic model in the flow field of front measuring tube, rear measuring tube, eight-slot nozzle, weld metal, and solid model of solid structure are obtained. As shown in Figure 6, the solid structure domain and flow field domain of the nozzle flowmeter. In Figure 6(b), the positions of the pressure taking orifice in the upstream and downstream of the eight-slot nozzle of the nozzle flowmeter are marked, respectively.

In this paper, ICEM software is used to mesh the fluid calculation domain and solid domain of the nozzle flowmeter. For the complex calculation domains such as the front measuring tube, the rear measuring tube, the eight-slot nozzle, and the weld metal basin, unstructured tetrahedral grids with good adaptability are used, and the hexahedral core is used in the interior. Among them, the grid number of the front measuring tube, the rear measuring tube, the eight-slot nozzle, and the weld metal basin are 63875, 63872, 1424041, and 38623, respectively, and the total grid number is 1590411. The total number of solid field grids is 100,000. As we know, the grid number plays an important role in characteristic prediction of the flowmeter. In this paper, several calculations with different grid numbers are carried out to observe the performance trend of flowmeter. When the final pressure difference of flowmeter is less than 2%, the effect of grid number could be thought that it is ignored. Meanwhile, the $y+$ value for the first cell on the surface of different parts of the nozzle flowmeter is near 30, the feature is able to satisfy the calculation requirement and accurately predict the flowmeter performance. The grid diagram of the whole flow field, middle section, and solid structure of nozzle flowmeter are shown in Figure 7.

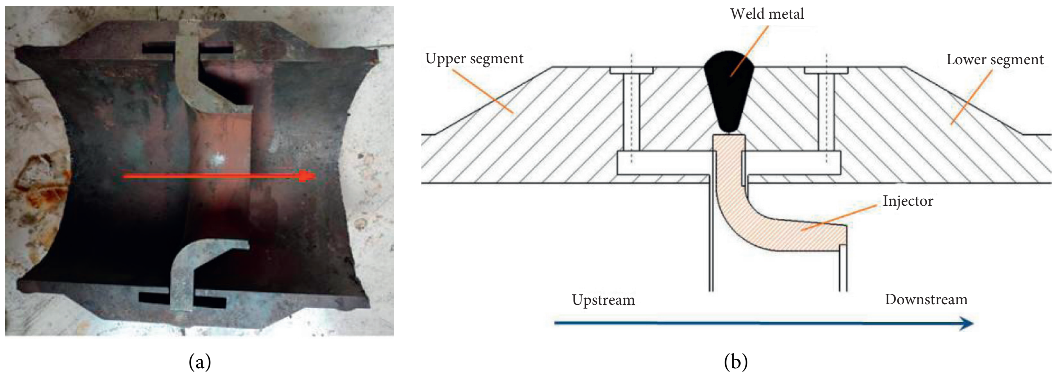

Figure 1: Overall structure. (a) Real products. (b) Basic structure.

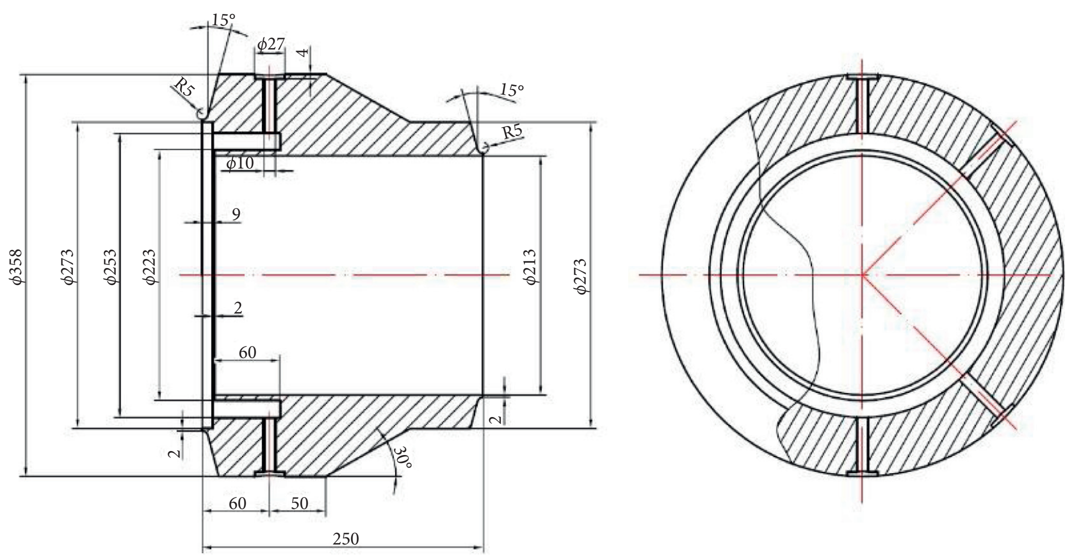

Figure 2: Measuring tube.

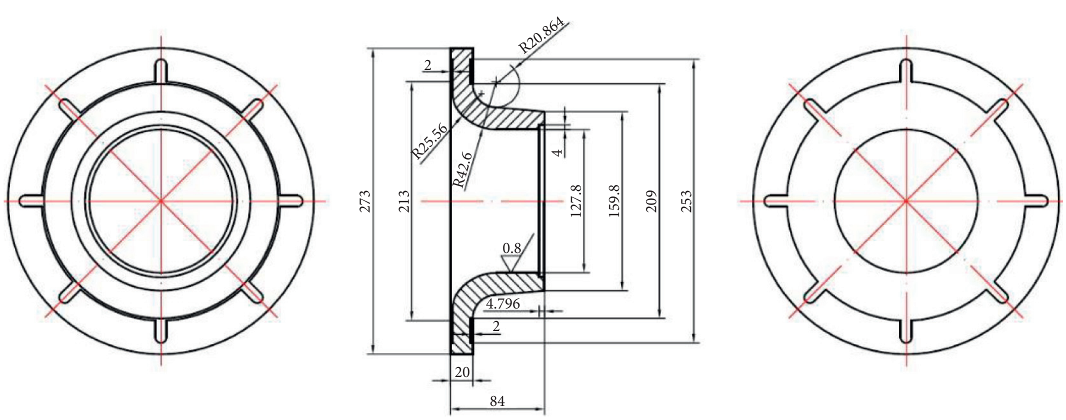

Figure 3: Eight-slot nozzle.

The grids number will not only affect calculation efficiency but also seriously affect the accuracy of numerical simulation. Therefore, it is crucial for numerical simulation to verify the independence of the grids number and select the appropriate grid scheme before calculation. In this paper, five different mesh models in fluid calculation domain are used, respectively, to verify the mesh independence of the pressure loss (Δp) of the nozzle flow meter and the pressure difference (Δp_n) of the pressure taking orifice in the upstream and downstream. The results are shown in Table 1.

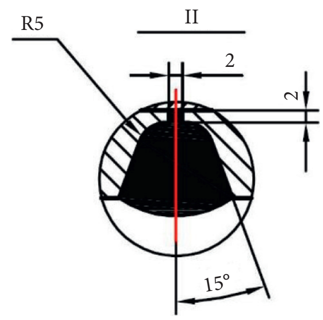

Figure 4: Weld metal.

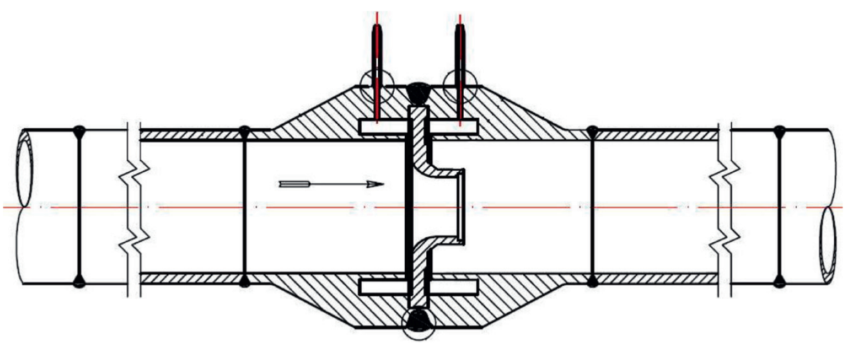

Figure 5: Two-dimensional drawing of nozzle flowmeter.

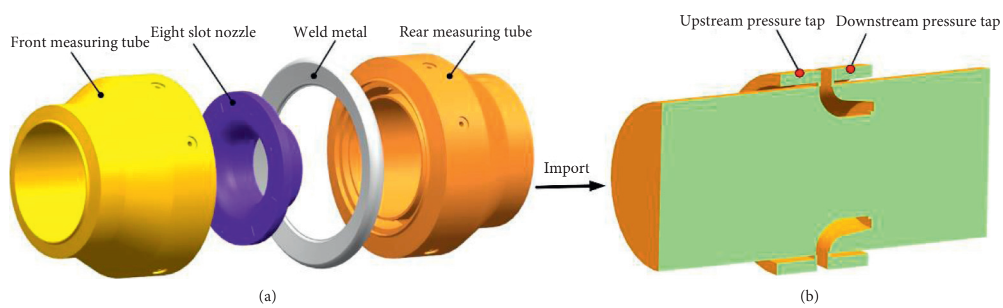

Figure 6: Schematic diagram of solid structure and flow field calculation domain. (a) Solid structure domain. (b) Half-section view of flow field.

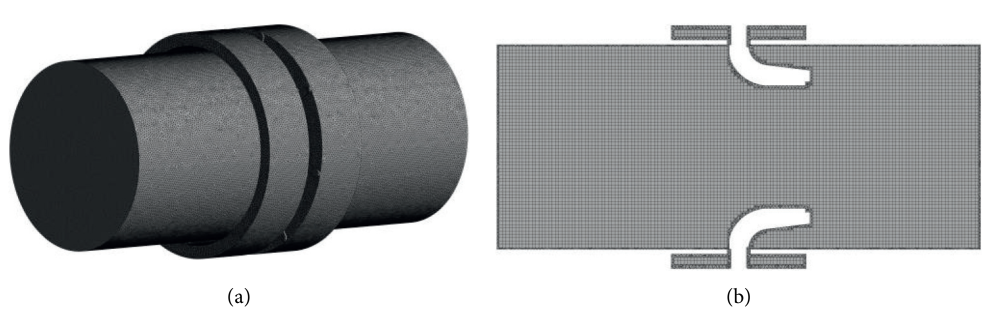

Figure 7: Continued.

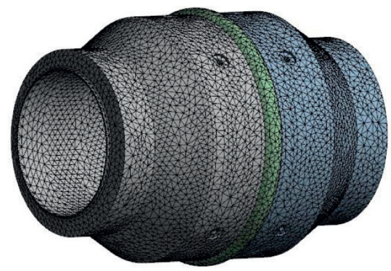

(c)

Figure 7: Flow field and rotor structure grid of flowmeter. (a) The whole flow field. (b) Cross-section grid in flow field. (c) Solid field domain grid.

Table 1: Grid information of flow field domain.

Scheme	Scheme 1	Scheme 2	Scheme 3	Scheme 4	Scheme 5
Grid number ($\times 10^4$)	48.1778	82.4195	110.7327	159.0411	182.8976
Pressure loss Δp (Pa)	1.4210124	1.4422614	1.54193002	1.5696321	1.55801269
Pressure difference Δp_n (Pa)	2.7000085	2.6934170	2.72725711	2.8020022	2.80326806

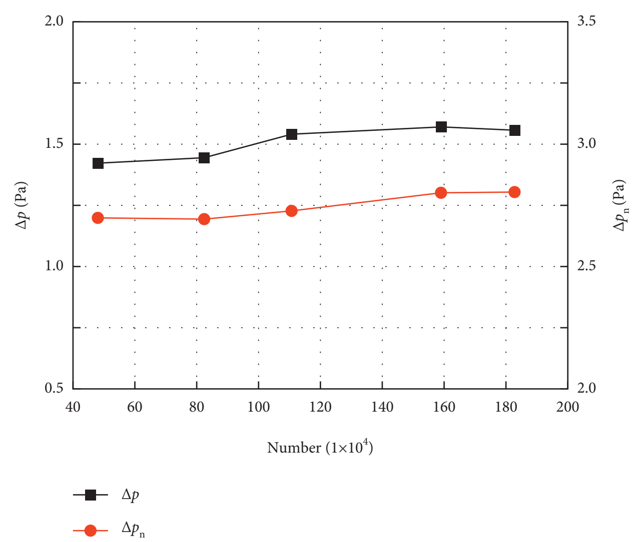

Figure 8: Grid independence verification results.

Figure 8 shows the relationship between the pressure loss of the nozzle flowmeter and the pressure difference between the pressure taking orifice in the upstream and downstream. It can be seen from Table 1 and Figure 8 that when the grid number in the flow domain exceeds 159.04×10^4, the measurement characteristics of the nozzle flowmeter are basically stable. Considering the efficiency and accuracy of the calculation, the grid number of flow field finally selected in this paper is 159.04×10^4.

4. Numerical Method

The numerical calculation of nozzle flowmeter includes the numerical simulation of flow field and solid field. The computational fluid dynamics software FLUENT and the solid field finite element analysis software ANSYS Workbench are used to numerically simulate the flow field and thermal effect of nozzle flowmeter at different inner wall temperatures. As we know, the standard k-ε turbulence model is suitable for most of common flow. Therefore, in this paper, the standard k-ε turbulence model is used to enclose the average Reynolds equation and to carry out the numerical calculation of internal flow inside the flowmeter. For the thermal analysis of the flowmeter, it is necessary to study the heat transfer mode in the flowmeter.

In recent years, the fluid-solid coupling method has been widely used to analyze the influence of fluid on the stress characteristics of solid structures. The coupling system of nozzle flowmeter has the characteristics of extremely unstable flow, small deformation of solid structure, and complex three-dimensional flow. In this paper, the iterative fluid-solid coupling method is used to calculate the fluid-solid coupling of the nozzle flowmeter. Iterative fluid-solid coupling methods mainly include bidirectional and unidirectional fluid-solid coupling methods. Among them, the bidirectional coupling calculation efficiency is low, and the calculation resource consumption is large. The unidirectional fluid-structure coupling is mainly applicable to the case that the solid structure is less affected by the flow field, and the deformation of the solid mechanism is less affected by the flow field. Compared with bidirectional coupling, the unidirectional coupling method not only has higher computational efficiency but also requires less computational resources. Because the nozzle flowmeter structure studied in this paper is less deformed by fluid force, the unidirectional fluid-solid coupling method is selected.

The medium is air, which is an incompressible fluid, and the density was set to be 1.293 kg/m^3. The inlet boundary condition is the velocity inlet, and the velocity value is converted according to different simulated flow rates. The outlet is free flow, and the extension of the outlet section ensures the full development of the fluid at the outlet. All solid walls are set to the standard wall boundary conditions, which are set to the stationary wall and the wall roughness is set to the smooth wall, and the function near the wall is the standard wall function. The coupling calculation between velocity and pressure is realized by SIMPLEC algorithm. The second order upwind scheme is adopted for the spatial discretization of convection term and the central difference scheme is adopted for the spatial discretization of diffusion term.

5. Results and Discussion

5.1. Measurement Characteristic Curve. Figure 9 shows the pressure loss variation curve of nozzle flowmeter under different flow rates. It can be seen that the pressure loss between the inlet and outlet of nozzle flowmeter increases with the increase of flow rate. When the flow rate is less than 250 m^3/h, the pressure loss of the flowmeter is less than 10 Pa, and the pressure loss increases little with the flow rate. When the flow rate is greater than 250 m^3/h, the growth rate of pressure loss obviously increases with the increase of flow rate. When the flow rate is 1000 m^3/h, the pressure loss reaches a large value of 125.24 Pa, and when the flow rate is 10 m^3/h, the pressure loss reaches a small value of 0.024 Pa.

Figure 10 shows the variation curve of pressure difference between upstream and downstream of nozzle flowmeter under different flow rates. It can be seen that the pressure difference between upstream and downstream of the nozzle flowmeter increases with the rising flow rate. When the flow rate is less than 250 m^3/h, the pressure difference is less than 25 Pa, and it increases little with the flow rate. When the flow rate is greater than 250 m^3/h, the growth rate of pressure difference increases significantly with the increase of flow rate. When the flow rate is 1000 m^3/h, the pressure difference reaches a large value of 281.75 Pa. When the flow rate is 10 m^3/h, the pressure difference reaches a small value, which is 0.03 Pa.

5.2. Temperature Field Analysis. Figures 11 and 12 shows the temperature field distribution of the cross section in the fluid domain at 50°C and 700°C of the inner wall temperature under different flow rates. It can be seen that when the outer wall temperature remains unchanged at 20°C, the internal heat transfer of the nozzle flowmeter gradually weakens with the increase of flow rate. When the flow rate rises from 10 m^3/h to 1000 m^3/h, the internal temperature field decreases with the increase of flow rate. When the flow rate is 10 m^3/h, the heat transfer in the fluid domain is obvious, the internal low temperature area is less, and the high temperature area extends to the outlet of the flowmeter. When the flow rate is 1000 m^3/h, the internal heat transfer phenomenon is weak, and the internal temperature distribution is mainly concentrated in the low temperature section.

5.3. Pressure Field Analysis. Figures 13 and 14 show the cross-sectional pressure distribution in the fluid domain with different inner wall surface temperatures at a flow rate of 10 m^3/h and 1000 m^3/h. It can be seen that the internal pressure distribution is similar when the outer wall surface temperature remains constant when temperature is 50°C, 100°C, 300°C, 500°C, and 1000°C. When the temperature of the inner wall surface rises from 50°C to 1000°C, the pressure field inside the fluid domain of the flowmeter shows a gradually decreasing distribution from the inlet to the outlet. This indicates that the nozzle flowmeter internal wall temperature has little effect on the fluid flow.

5.4. Equivalent Dynamic Stress Analysis. Considering the influence of fluid domain changes on the structural field, this paper analyzes the structural characteristics of the nozzle flowmeter under different flow rates and inner wall temperature based on the single-phase fluid-solid coupling calculation method. The concept of equivalent dynamic stress is introduced in the analysis of dynamic stress based on the fourth strength theory, and the expression of its equivalent dynamic stress σ_{eq} (Von Mises stress) is

$$\sigma_{eq} = \sqrt{\frac{1}{2}\left[\left(\sigma_x - \sigma_y\right)^2 + \left(\sigma_y - \sigma_z\right)^2 + \left(\sigma_z - \sigma_x\right)^2\right]}, \qquad (2)$$

where σ_x, σ_y, and σ_z denote the first, second, and third principal stresses, respectively. Figures 15 and 16 show the dynamic stress distribution diagram of the flowmeter with different inner wall surface temperatures under 10 m^3/h and 1000 m^3/h. It can be seen that when the outer wall surface temperature remains constant when the nozzle flowmeter internal wall surface temperature is 50°C, 100°C, 300°C, 500°C, and 1000°C, the internal dynamic stress is similar. When the temperature of the inner wall surface rises from 50°C to 1000°C, the high dynamic stress region inside the fluid domain of the flowmeter all appears at the inlet and outlet of the eight-slot nozzle, but its value is still low, which is 0.245 Pa. This also indicates that the nozzle flowmeter internal wall temperature has little effect on the flowmeter dynamic stress.

5.5. Fluid-Induced Vibration Deformation Analysis. Changes in the fluid domain of the flowmeter will deform the structure of the flowmeter. This phenomenon is the

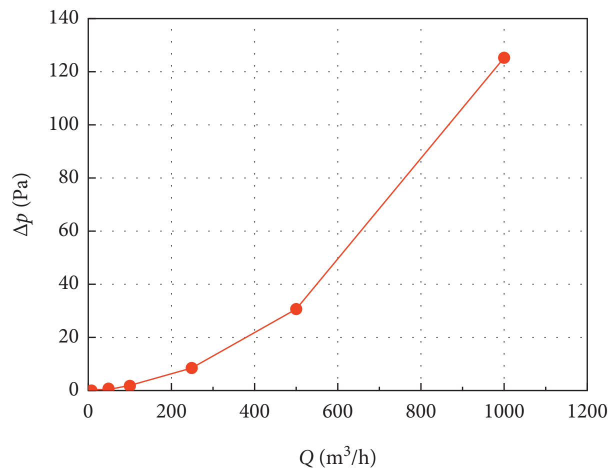

Figure 9: Pressure loss curve of nozzle flowmeter.

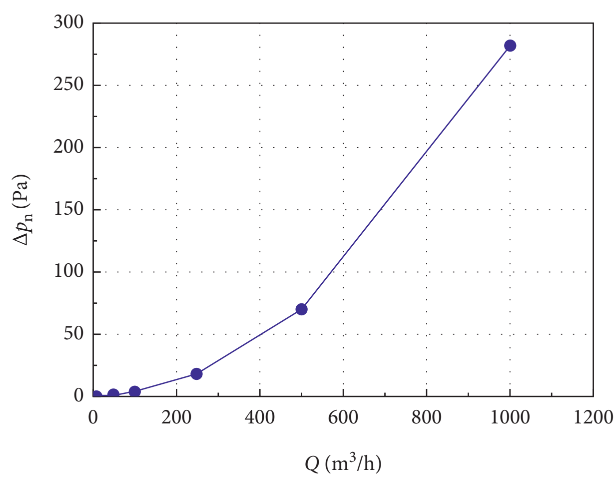

Figure 10: Pressure difference of upstream and downstream nozzle.

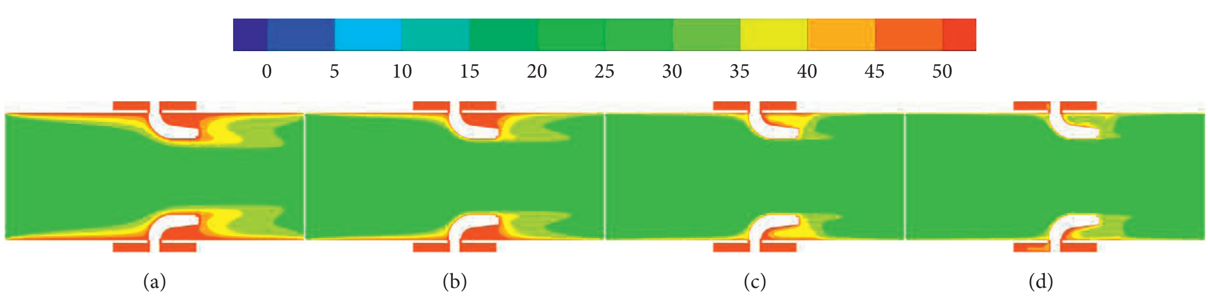

Figure 11: Temperature field distribution in fluid domain at 50°C. (a) 10 m^3/h. (b) 100 m^3/h. (c) 500 m^3/h. (d) 1000 m^3/h.

phenomenon of fluid-induced vibration. Based on the single-phase fluid-solid coupling calculation method, this paper analyzes the phenomenon of fluid-induced vibration deformation of the nozzle flowmeter at different flow rates and inner wall temperature. Figures 17 and 18 show the fluid-induced vibration of flowmeter with different inner wall surface temperature at a flow rate of 10 m^3/h and 1000 m^3/h. It can be seen that when the outer wall surface temperature remains constant when the nozzle flowmeter internal wall surface temperature is 50°C, 100°C, 300°C, 500°C, and 1000°C, the internal fluid-induced vibration is similar. When the temperature of the inner wall surface rises from 50°C to 1000°C, the high deformation areas inside the fluid domain of the flowmeter all appear at the inlet and outlet of the eight-slot nozzle, but its value is still low, which is 0.0017 μm. This indicates that the nozzle flowmeter internal wall surface temperature on the impact of vibration displacement generated by the fluid is small.

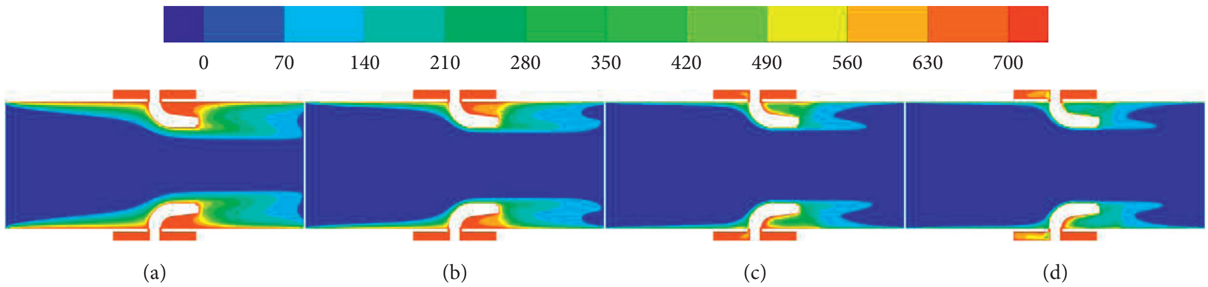

Figure 12: Temperature field distribution in fluid domain at 700°C. (a) 10 m^3/h. (b) 100 m^3/h. (c) 500 m^3/h. (d) 1000 m^3/h.

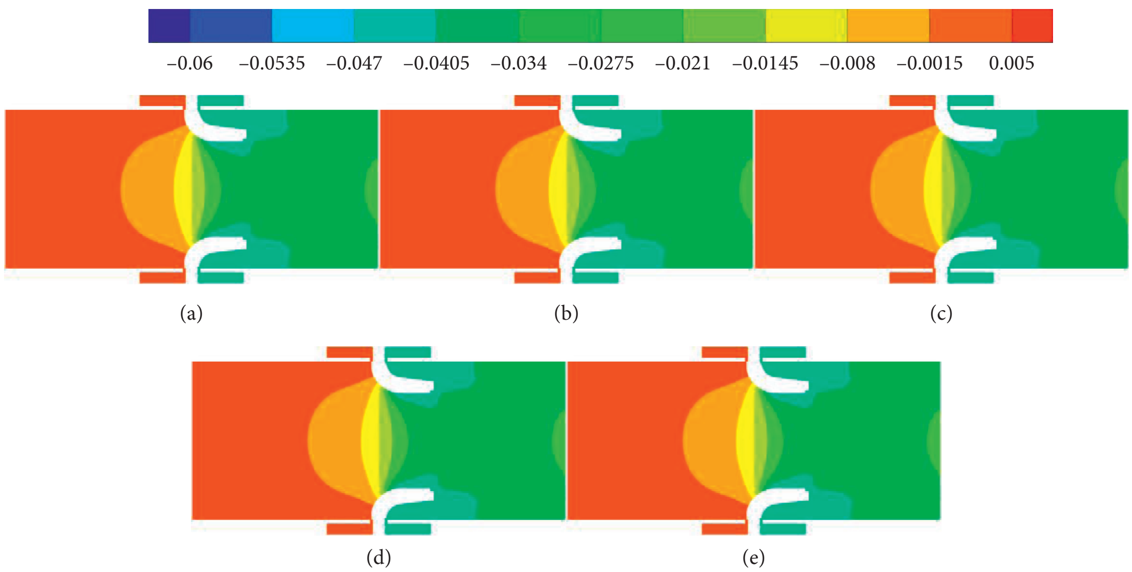

Figure 13: Pressure field distribution of cross section in flow meter (10 m^3/h). (a) 50°C. (b) 100°C. (c) 300°C. (d) 500°C. (e) 700°C.

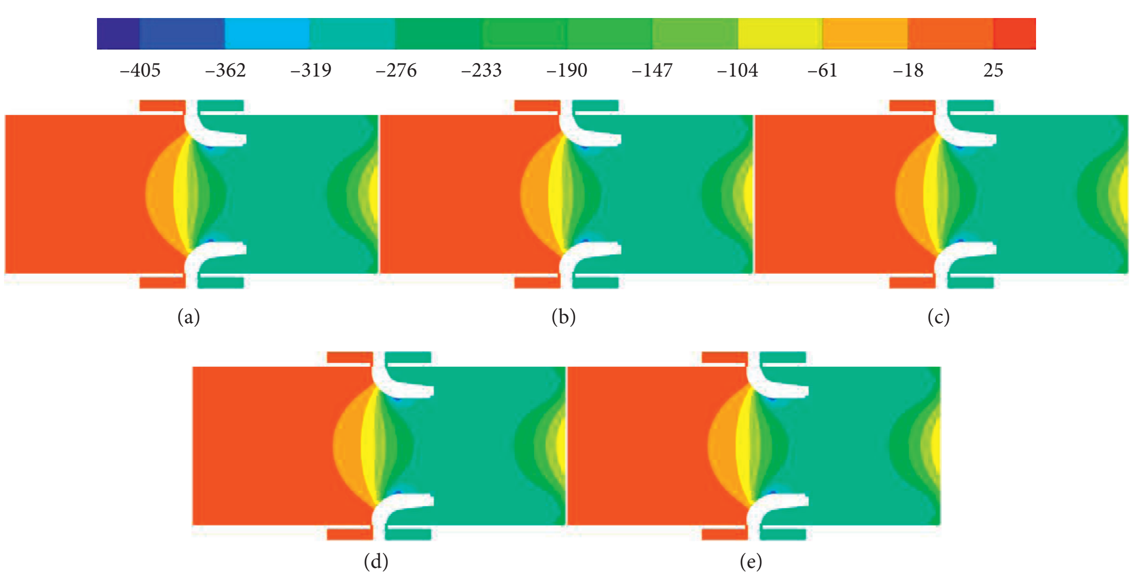

Figure 14: Pressure field distribution of cross section in flow meter (1000 m^3/h). (a) 50°C. (b) 100°C. (c) 300°C. (d) 500°C. (e) 700°C.

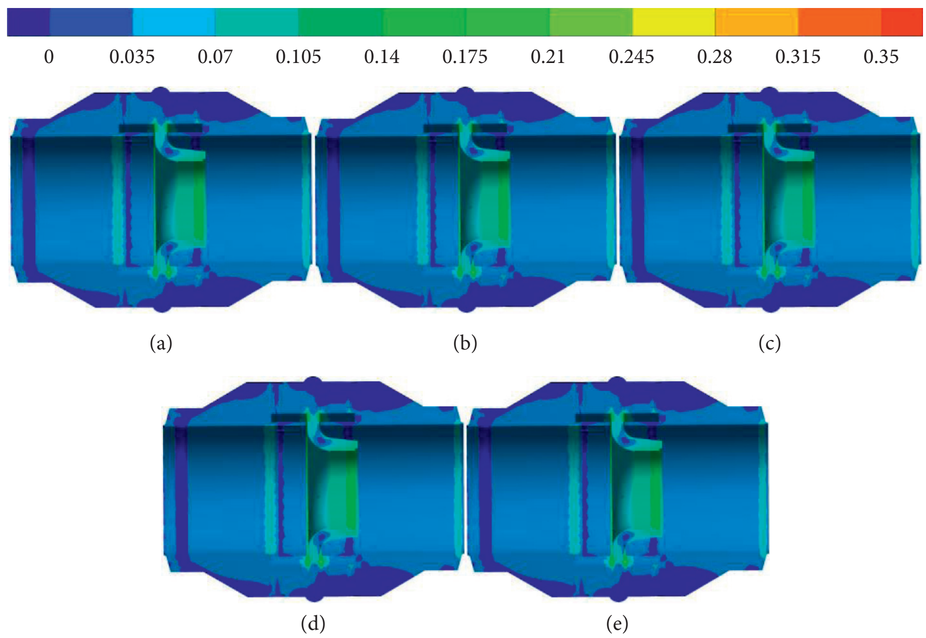

Figure 15: Dynamic stress distribution of cross section in flow meters (10 m^3/h). (a) 50°C. (b) 100°C. (c) 300°C. (d) 500°C. (e) 700°C.

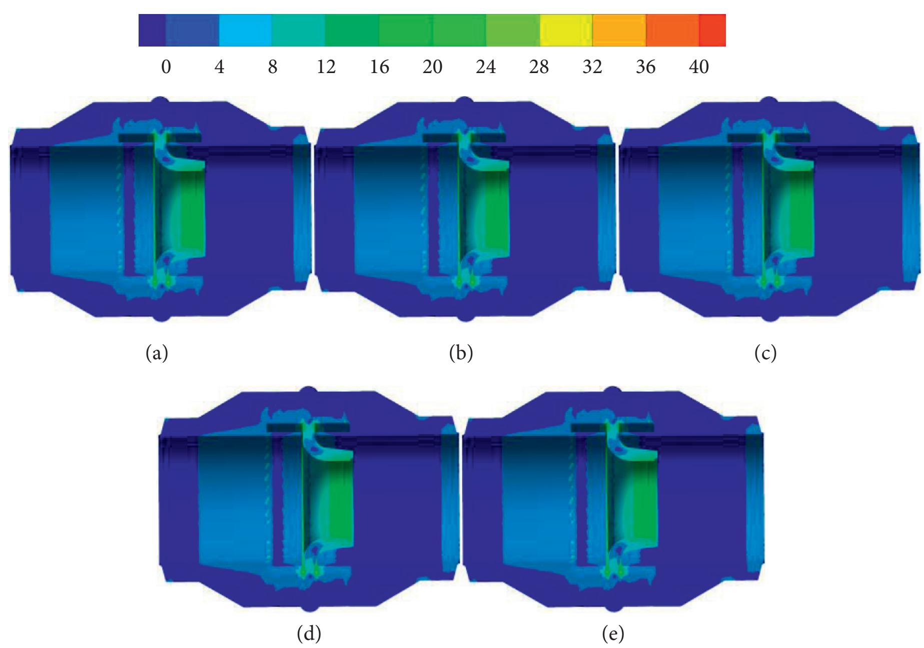

Figure 16: Dynamic stress distribution of cross section in flow meters (1000 m^3/h). (a) 50°C. (b) 100°C. (c) 300°C. (d) 500°C. (e) 700°C.

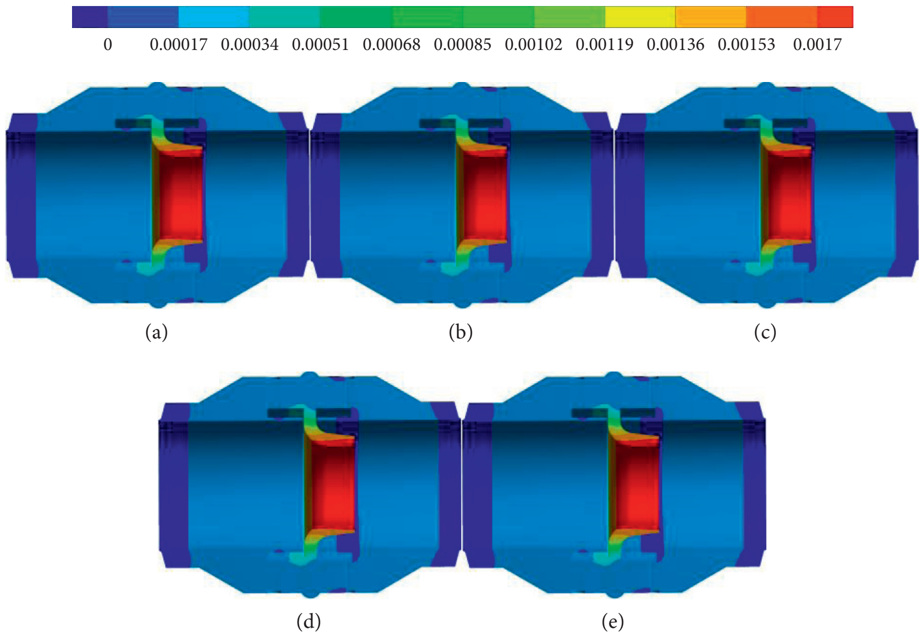

Figure 17: Deformation distribution in the section of fluid excitation (10 m^3/h). (a) 50°C. (b) 100°C. (c) 300°C. (d) 500°C. (e) 700°C.

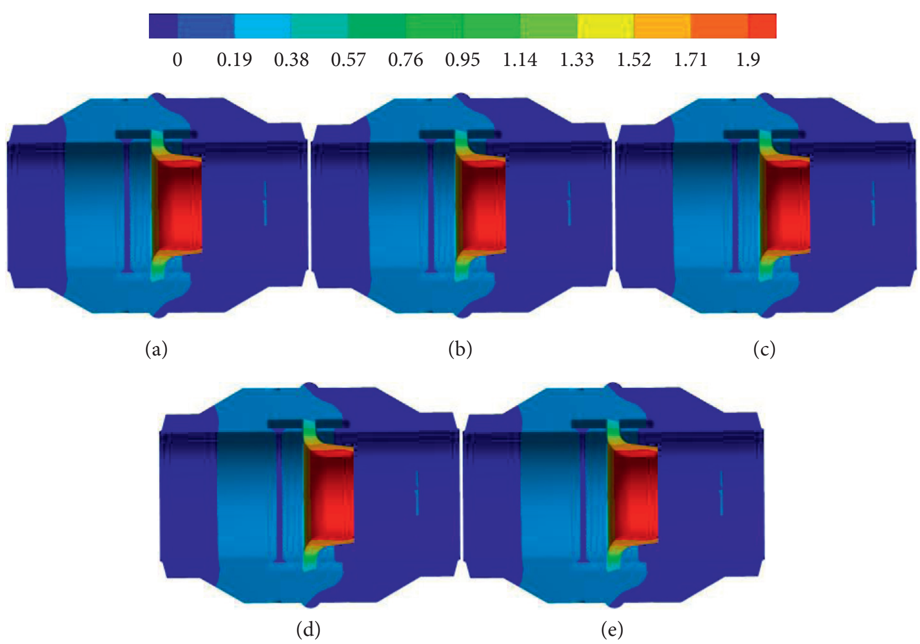

Figure 18: Deformation distribution in the section of fluid excitation (1000 m^3/h). (a) 50°C. (b) 100°C. (c) 300°C. (d) 500°C. (e) 700°C.

6. Conclusion

The heat transfer effect of the flowmeter decreases with the increase of flow rate and different inner wall temperature. Different inner wall surface temperatures have little effect on the pressure distribution of the flowmeter fluid domain and on the dynamic stress and fluid-induced vibration deformation.

Abbreviations

Q: Volume flow rate
H: Pump head
n: Rotational speed
s: Distance from hub
b: Blade number
t: Time

p: Total pressure at blade surface
ρ: Density of the fluid
u: Circumferential velocity
0: Before regulating flowrate
2: Impeller outlet.

Data Availability

The data used to support the findings of this study are available from the corresponding author upon request.

Conflicts of Interest

The authors declare no potential conflicts of interest with respect to the research, authorship, and/or publication of this article.

Authors' Contributions

Liang-Huai Tong and Yan-Juan Zhao carried out the numerical simulation and wrote the manuscript; Su-Lu Zheng and Yu-Liang Zhang analyzed the flow characteristics; Kai-Yuan Zhang and Jin-Fu Li checked the manuscript and revised it. All authors have read and agreed to the published version of the manuscript.

Acknowledgments

The research was financially supported by the National Natural Science Foundation of China (Grant no. 51876103) and Zhejiang Provincial Natural Science Foundation of China (Grant no. LZY21E060001).

References

[1] B. Min and B. E. Logan, "Continuous electricity generation from domestic wastewater and organic substrates in a flat plate microbial fuel cell," *Environmental Science & Technology*, vol. 38, no. 21, pp. 5809–5814, 2004.

[2] J. G. Yin and J. Li, "Discussion on site detection technology of steam flowmeter," *Metrology & Measurement Technique*, vol. 43, no. 1, pp. 48–50, 2016.

[3] Z. P. Hu and Y. Zhao, "Comparison of verification results of vortex flowmeter on different gas flow standard devices," *China Metrology*, vol. 9, pp. 59-60, 2007.

[4] L. Z. Huang, "Gas flow standard device with sonic nozzles," *China Measurement & Test*, vol. 31, no. 3, pp. 50–52, 2005.

[5] L. Zhao, M. L. Zhang, and X. H. Xu, "Application and research of critical flow venturi nozzle method in gas flowmeter verification," *China Instrumentation*, vol. 6, pp. 33–37, 2002.

[6] Z. Pan, B. D. Chen, Y. F. Yan, and L. Y. Shang, "Numerical simulation of surface pressure distribution of V-cone flowmeter," *Energy Conservation Technology*, vol. 27, no. 4, pp. 299–301, 2009.

[7] S. Guo, H. Okamoto, and Y. Maruta, "Measurement on the fluid forces induced by rotor-stator interaction in a centrifugal Pump," *JSME International Journal Series B*, vol. 49, no. 2, pp. 434–442, 2006.

[8] F. Zhang, F. Dong, and C. Tan, "High GVF and low pressure gas-liquid two-phase flow measurement based on dual-cone flowmeter," *Flow Measurement and Instrumentation*, vol. 21, no. 3, pp. 410–417, 2010.

[9] D. S. Chen, B. L. Cui, and Z. C. Zhu, "Internal flow characteristics and aft-cone angle on performance of swirlmeter," *Mapan*, vol. 31, no. 2, pp. 107–113, 2016.

[10] D. Chen, B. Cui, and Z. Zhu, "Research on internal flow and performance of swirlmeter with different swirler cone angle," *Measurement and Control*, vol. 49, no. 4, pp. 136–142, 2016.

[11] K. Perumal and J. Krishnan, "A CFD study of the effect of venturi geometry on high pressure wet gas metering," *International Journal of Oil, Gas and Coal Technology*, vol. 6, no. 5, pp. 549–566, 2013.

[12] K. Perumal and S. M. San, "CFD study of the effect of venture convergent and divergent angles on low pressure wet gas metering," *Journal of Applied Sciences*, vol. 14, no. 22, pp. 3036–3045, 2014.